HAL open science

Achieving Higher Levels of Crack Simulation with the Improved Adaptive Static Condensation Method

Ali Mezher, Ludovic Jason, Gauthier Folzan, Luc Davenne

To cite this version:

Ali Mezher, Ludovic Jason, Gauthier Folzan, Luc Davenne. Achieving Higher Levels of Crack Simulation with the Improved Adaptive Static Condensation Method. Buildings, 2024, 14 (3), 10.3390/buildings14030648 . hal-04485175

HAL Id: hal-04485175

https://hal.science/hal-04485175v1

Submitted on 1 Mar 2024

HAL is a multi-disciplinary open access archive for the deposit and dissemination of scientific research documents, whether they are published or not. The documents may come from teaching and research institutions in France or abroad, or from public or private research centers.

L'archive ouverte pluridisciplinaire **HAL**, est destinée au dépôt et à la diffusion de documents scientifiques de niveau recherche, publiés ou non, émanant des établissements d'enseignement et de recherche français ou étrangers, des laboratoires publics ou privés.

Autorisation HAL

HAL Authorization

buildings

MDPI

Article

Achieving Higher Levels of Crack Simulation with the Improved Adaptive Static Condensation Method

Ali Mezher [1,2,*], Ludovic Jason [1], Gauthier Folzan [1] and Luc Davenne [2]

[1] CEA, Service d'Études Mécaniques et Thermiques, Université Paris-Saclay, 91191 Gif-sur-Yvette, France; ludovic.jason@cea.fr (L.J.); gauthier.folzan@cea.fr (G.F.)
[2] LEME, UPL, Université Paris Nanterre, 92410 Ville d'Avray, France; luc.davenne@parisnanterre.fr
* Correspondence: ali.mezher@cea.fr

Abstract: Accurately simulating concrete cracking in large-dimensional structures is a challenging task. To address this issue, an adaptive static condensation (ASC) method has been developed that has demonstrated effectiveness in localized nonlinearities. The ASC method aims to concentrate computational efforts solely on the damaged area, which may evolve due to crack initiation or propagation. However, the efficiency of the ASC method may be limited as it is based on a non-evolving mesh. To overcome this limitation, a novel approach is proposed in this study, which utilizes an evolutionary mesh with mesh refinement. The proposed approach employs a fine mesh solely in the activated and evolving domain of interest. The ASC method with mesh refinement is demonstrated on a notched bending beam, indicating that the accuracy of the ASC is maintained while providing an additional gain in computational time. Furthermore, a reinforced concrete vessel subjected to internal pressure is considered, and it is shown that this new approach results in a significant improvement in computational time, with a 14-fold improvement compared to a 5-fold improvement without mesh refinement. This study demonstrates that the proposed improvement on the ASC method allows for finer discretization in the zones of interest that were previously inaccessible with the nominal ASC method or a direct numerical simulation strategy.

Keywords: adaptive static condensation; mesh refinement; large-scale structures; crack

check for updates

Citation: Mezher, A.; Jason, L.; Folzan, G.; Davenne, L. Achieving Higher Levels of Crack Simulation with the Improved Adaptive Static Condensation Method. *Buildings* **2024**, *14*, 648. https://doi.org/10.3390/buildings14030648

Academic Editor: Hugo Santos

Received: 18 January 2024
Revised: 15 February 2024
Accepted: 19 February 2024
Published: 29 February 2024

Copyright: © 2024 by the authors. Licensee MDPI, Basel, Switzerland. This article is an open access article distributed under the terms and conditions of the Creative Commons Attribution (CC BY) license (https://creativecommons.org/licenses/by/4.0/).

1. Introduction

Performing nonlinear simulations on large-scale structures using fine meshes is a significant industrial challenge due to the rapid scaling of computational costs with increasing mesh refinement. For instance, simulating the mechanical behavior of a containment vessel with a required element size of approximately one centimeter to accommodate regularization models would result in more than 10^{10} degrees of freedom (dof), given the structure's dimensions of 37 m in diameter and 60 m in height. The high number of dof, along with the use of nonlinear models, poses a significant challenge for simulating such cases on current machines. Thus, alternative methods that can handle such complexities are necessary.

This paper focuses on the concrete cracking behavior of large reinforced and prestressed concrete structures. To model localized cracking accurately, a nonlinear constitutive law and a fine mesh are necessary. A commonly employed method in the literature to improve computational performance is parallel processing. This method utilizes multiple computer cores to simultaneously solve multiple operations. With the advent of massive computational capacities in recent decades, researchers have been able to increase simulation complexity while also significantly reducing computation time through the use of parallel computing. The utilization of parallel computing has been observed in various domains such as finance [1] and fluid mechanics [2]. Parallel computing relies on domain decomposition methods, which are now mature mathematical techniques for the resolution of large algebraic systems formulated using finite element models on parallel computers [3].

In 1991, Farhat and Roux [4] proposed the finite element tearing and Interconnecting (FETI) method as a domain decomposition technique for solving static problems with less inter-processor communication compared to other methods. While FETI is efficient for regular geometries and homogeneous materials, it may not be suitable for structures with complex geometries or heterogeneous material properties. An alternative approach is the adaptive mesh refinement (AMR) method, which utilizes locally adapted discretization for better accuracy and computational efficiency. In this method, a fine mesh is employed in areas where the solution is complex, while a coarser mesh is used in other areas. The AMR method allows for the mesh to be adaptively refined or de-refined in space and time during the simulation. Originally proposed in [5] for solving hyperbolic partial differential equations, an adaptive version of 2D mesh refinement for conservation laws was later introduced in [6]. Several works have extended the concept of AMR to applications that involve elliptic and parabolic equations, as well as non-hyperbolic regimes [7]. AMR techniques have become an essential tool for many scientific applications and have been applied in a variety of fields ranging from geophysical fluid dynamics simulations [8] to relativistic astrophysical flows [9], nonlinear elastodynamics [10], and fluid dynamics and solid mechanics (including combustion) [11,12]. The AMR approach is advantageous in terms of its performance with respect to memory size and CPU time [13]. However, the AMR approach still models the entire structure, which is computationally sub-optimal and particularly inefficient when the area of interest is small compared to the entire structure. Moreover, the transfer of mechanical state from one mesh to another during refinement requires complex operations in cases of strong nonlinearities, potentially leading to precision errors that limit the method's use. In computational mechanics, the static condensation method [14] is a model reduction technique that eliminates unknowns from the linear system in the stiffness matrix, thus reducing the number of degrees of freedom. This creates condensed sub-structures, or "super-elements", which are typically defined by removing internal unknowns in the condensed zones. The static condensation method is suitable for complex problems and has been widely used in mechanics since its introduction by Guyan in 1965. While the method is only exact for static problems, it has been used in structural dynamics, where the condensation of mass is approximated. The method has been improved over time for dynamic calculations ([15,16]) and has been combined with sub-structuring in the analysis of structures with localized nonlinearities [17].

Regarding nonlinear cracking in reinforced concrete structures, a so-called "Adaptive Static Condensation (ASC)" method has been developed in recent years [18,19]. This method is specifically designed to handle large structures that exhibit local nonlinear behavior that can evolve over time. The ASC method is based on the principle of static condensation and involves partitioning the structure into zones based on a linear pre-computation. The zones with expected nonlinear behavior are then fully represented, while the zones with linear elastic behavior are condensed. During the calculation, the condensed zones are checked to ensure that they remain elastic. If non-elastic behavior is detected, new areas of interest are included and fully represented in the calculation. However, the efficiency of the ASC method may be limited if the damage spreads over a large part of the structure early in the computation. Despite this limitation, the ASC method has shown promising results in classical applications.

In its original form, the ASC method is designed for use on a non-evolving mesh. However, to accurately simulate structural problems that involve non-local damage models, a fine mesh of the entire structure is often required. This can impede the performance of the ASC calculation or even render it impossible due to the pre-computation steps that are applied to the entire mesh. As a result, modifications have been made to the original method to address this limitation. These modifications involve keeping the initial mesh on which the preparation phases are performed as coarse as possible, while refining the evolving domain of interest on which the nonlinear calculation is performed until a target mesh refinement is achieved.

The current paper commences with a presentation of an improved version of the ASC method, which involves mesh refinement of the domain of interest in Section 2.1. The method is subsequently applied to a notched bending beam in two dimensions, where its effectiveness is verified, in Section 2.4. Additionally, the paper presents an application of the method on a simplified reinforced concrete containment vessel, which is subjected to an internal pressure in three dimensions. An analysis is conducted in Sections 2.5 and 2.6 to determine the impact of mesh size on the calculation results.

2. Adaptive Static Condensation Improved by Mesh Refinement

The ASC method is based on a zoning technique that involves partitioning a given structure into two types of zones: Zones of interest, where nonlinear simulations are performed, and condensed zones, where an elastic behavior is expected. The main objective of the ASC method is to optimize the computational effort of nonlinear calculations by focusing on the predefined "zones of interest", which are anticipated to exhibit cracking behavior, while "condensing" the zones with a linear elastic behavior. This is achieved through the application of static condensation [14] to replace the elastic zones with equivalent boundary conditions applied at the boundaries of the zones of interest. As the structure evolves, due to the propagation of a given crack or the initiation of a new one, specific criteria are used to identify whether damage is likely to occur, which leads to changes in the geometry of the zones of interest. The ASC method reduces the computational domain of the nonlinear problem without compromising the quality of the results compared to a reference nominal computation of the entire structure. This section provides an overview of the theoretical principles of the ASC method using two-level static condensation, followed by a detailed description of the ASC algorithm, including mesh refinement.

2.1. ASC: Two Level Guyan's Static Condensation

Static condensation allows, in the case of linear elasticity, to find the exact solution of the system on only a chosen part of the structure by eliminating the dof of the rest of the structure. For a given mechanical problem discretized with n dof, the static equilibrium can be expressed by the following equation:

$$K\,U = F \tag{1}$$

where K represents the stiffness matrix of the structure, u is the displacement vector and F the nodal force vector. The number of dof of the static equilibrium problem is the dimension of the displacement vector U. Guyan's approach consists in decomposing the structure into two domains called: The domain of interest (DI) and the elastic domain. These domains have dof which are noted N^I for the DI and N^E for the elastic domain. The sets N^I and N^E intersect, and certain dof, denoted N^Γ, belong to both domains. N_v^I and N_v^E are the dof strictly internal to the DI, respectively, to the elastic domain. The system of Equation (1) can be rewritten as:

$$\begin{pmatrix} K_{vv}^E & K_{v\Gamma}^E & 0 \\ K_{\Gamma v}^E & K_{\Gamma\Gamma}^E + K_{\Gamma\Gamma}^I & K_{\Gamma v}^I \\ 0 & K_{v\Gamma}^I & K_{vv}^I \end{pmatrix} \begin{pmatrix} U_v^E \\ U_\Gamma \\ U_v^I \end{pmatrix} = \begin{pmatrix} F_v^E \\ F_\Gamma \\ F_v^I \end{pmatrix} \tag{2}$$

The index "v" designates the rows or columns corresponding to the dof of the internal "volume" and the index "Γ" designates the rows or columns corresponding to the dof located on the interface. The parameters of Equation (2) are therefore:

K_{vv}^E: the stiffness terms relative to the internal dof of the elastic domain

$K_{v\Gamma}^E$: the stiffness terms relative to the internal–boundary connections of the elastic domain

$K_{\Gamma v}^E$: the stiffness terms relative to the boundary–internal connections of the elastic domain

$K^E_{\Gamma\Gamma}$: the stiffness terms relative to the boundary–boundary connections of the elastic domain
K^I_{vv}: the stiffness terms relative to the internal dof of the DI
$K^I_{v\Gamma}$: the stiffness terms relative to the internal–boundary connections of the DI
$K^I_{\Gamma v}$: the stiffness terms relative to the boundary–internal connections of the DI
$K^I_{\Gamma\Gamma}$: the stiffness terms relative to the boundary–boundary connections of the DI
U^E_v, F^E_v: respectively the displacement vector and the force vector in the elastic domain.
U_Γ, F_Γ: respectively the displacement vector and force vector on the interface Γ.
U^I_v, F^I_v: respectively the displacement vector and the force vector in the DI.
The expansion of system (2) gives:

$$\begin{cases} K^E_{vv}U^E_v + K^E_{v\Gamma}\,U_\Gamma = F^E_v & \text{(3a)} \\ K^E_{\Gamma v}U^E_v + (K^E_{\Gamma\Gamma} + K^I_{\Gamma\Gamma})U_\Gamma + K^I_{\Gamma v}U^I_v = F_\Gamma & \text{(3b)} \\ K^I_{\Gamma v}U_\Gamma + K^I_{vv}U^I_v = F^I_v & \text{(3c)} \end{cases}$$

Equation (3a) can be written:

$$U^E_v = {K^E_{vv}}^{-1}\left(F^E_v - K^E_{v\Gamma}\,U_\Gamma\right) \tag{4}$$

The static condensation consists in replacing Equation (4) in the last two equations of system (3) and allows to write:

$$\begin{cases} \begin{pmatrix} \hat{K}^E_{\Gamma\Gamma} + K^I_{\Gamma\Gamma} & K^I_{\Gamma v} \\ K^I_{v\Gamma} & K^I_{vv} \end{pmatrix} \begin{pmatrix} U_\Gamma \\ U^I_v \end{pmatrix} = \begin{pmatrix} \hat{F}_\Gamma \\ F^I_v \end{pmatrix} & \text{(5a)} \\ U^E_v = {K^E_{vv}}^{-1}(F^E_v - K^E_{v\Gamma}\,U_\Gamma) & \text{(5b)} \end{cases}$$

where:

$$\begin{cases} \hat{K}^E_{\Gamma\Gamma} = K^E_{\Gamma\Gamma} - K^E_{\Gamma v}\,{K^E_{vv}}^{-1}K^E_{v\Gamma} \\ \hat{F}_\Gamma = f_\Gamma - K^E_{\Gamma v}\,{K^E_{vv}}^{-1}\,F^E_v \end{cases}$$

Solving (5) is conducted by:

- calculation of ${K^E_{vv}}^{-1}$ first;
- resolution of Equation (5a);
- then, if necessary, calculation of U^E_v using the Equation (5b).

Guyan's approach therefore allows to write the system in such a way as to find the solution to the problem associated with the DI only by "condensing" the elastic domain. However, it remains possible to obtain the solution in the elastic domain by solving Equation (5b) ("decondensation"). Note that if the elastic domain is large, the dimension of the term K^E_{vv} is large, and the calculation of its inverse can become costly. It should be noted here that the matrix $\hat{K}^E_{\Gamma\Gamma}$ can be dense, and this reduced system can become difficult to solve. Storing the full condensed matrix can also be more expensive than the full sparse matrix. Even with these factors, the resolution of this reduced system remains faster than that of the global system, particularly when the condensed part is large compared to the non-condensed one. The ASC is an evolutionary method, which means that the DI can evolve several times during the calculation. At each evolution, it is necessary to recalculate ${K^E_{vv}}^{-1}$ which can be very expensive. In order to optimize this operation, a two-level condensation, as shown in Figure 1, is used in the ASC method. It is assumed that the elastic domain is composed of J zones Z_j. The dof of each zone are separated into 3 parts:

- N^j_v: dof strictly internal to Z_j
- $N^j_{\gamma_j}$: dof on the boundary γ_j of Z_j but not on the border Γ of the domain of interest (Figure 1a).
- N^j_Γ: dof of Z_j which are on Γ (Figure 1b).

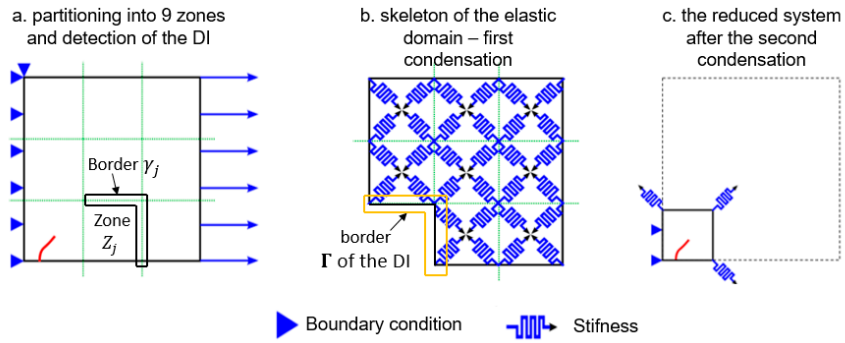

Figure 1. Illustration of the two-level condensation.

Potentially N^j_Γ or $N^j_{\gamma_j}$ can be empty if there is no intersection between Z_j and Γ or if the entire boundary of Z_j is in Γ. The union of all the zone boundaries forms a "skeleton" of the elastic domain $\gamma = \bigcup_j \gamma_j$.

The global system (1) is written with this decomposition as follows:

$$\begin{pmatrix} K^1_{vv} & 0 & \cdots & \cdots & 0 & K^1_{v\gamma} & K^1_{v\Gamma} & 0 \\ 0 & \ddots & & & \vdots & \vdots & \vdots & \vdots \\ \vdots & & K^j_{vv} & & \vdots & K^j_{v\gamma} & K^j_{v\Gamma} & \vdots \\ \vdots & & & \ddots & 0 & \vdots & \vdots & \vdots \\ 0 & \cdots & \cdots & 0 & K^J_{vv} & K^J_{v\gamma} & K^J_{v\Gamma} & \vdots \\ K^1_{\gamma v} & \cdots & K^j_{\gamma v} & \cdots & K^J_{\gamma v} & \sum_j K^j_{\gamma\gamma} & \sum_j K^j_{\gamma\gamma} & 0 \\ K^1_{\Gamma v} & \cdots & K^j_{\Gamma v} & \cdots & K^J_{\Gamma v} & \sum_j K^j_{\gamma\gamma} & \sum_j K^j_{\Gamma\Gamma} + K^I_{\Gamma\Gamma} & K^I_{\Gamma v} \\ 0 & \cdots & \cdots & \cdots & \cdots & 0 & K^I_{v\Gamma} & K^I_{vv} \end{pmatrix} \begin{pmatrix} U^1_v \\ \vdots \\ U^j_v \\ \vdots \\ U^J_v \\ U_\gamma \\ U_\Gamma \\ U^I_v \end{pmatrix} = \begin{pmatrix} F^1_v \\ \vdots \\ F^j_v \\ \vdots \\ F^J_v \\ F_\gamma \\ F_\Gamma \\ F^I_v \end{pmatrix} \tag{6}$$

Each zone is then condensed on its border by writing:

$$U^j_v = {K^j_{vv}}^{-1} \left(F^j_v - K^j_{v\gamma}\, U_\gamma - K^j_{v\Gamma}\, U_\Gamma \right) \qquad \forall j \tag{7}$$

Using Equation (7), Equation (6) can be re-written with the following system:

$$\begin{cases} \begin{pmatrix} \sum_j \hat{K}^j_{\gamma\gamma} & \sum_j \hat{K}^j_{\gamma\Gamma} & 0 \\ \sum_j \hat{K}^j_{\Gamma\gamma} & \sum_j \hat{K}^j_{\Gamma\Gamma} + K^I_{\Gamma\Gamma} & K^I_{\Gamma v} \\ 0 & K^I_{v\Gamma} & K^I_{vv} \end{pmatrix} \begin{pmatrix} U_\gamma \\ U_\Gamma \\ U^I_v \end{pmatrix} = \begin{pmatrix} \hat{F}_\gamma \\ \hat{F}_\Gamma \\ F^I_v \end{pmatrix} & \begin{matrix} \text{(8a)} \\ \\ \text{(8b)} \end{matrix} \\ U^j_v = {K^j_{vv}}^{-1} \left(F^j_v - K^j_{v\gamma}\, U_\gamma - K^j_{v\Gamma}\, U_\Gamma \right) \qquad \forall j \end{cases}$$

where:

$$\hat{K}^j_{\gamma\gamma} = K^j_{\gamma\gamma} - K^j_{\gamma v}\ {K^j_{vv}}^{-1} K^j_{v\gamma}$$

$$\hat{K}^j_{\gamma\Gamma} = K^j_{\gamma\Gamma} - K^j_{\gamma v}\ {K^j_{vv}}^{-1} K^j_{v\Gamma}$$

$$\hat{K}^j_{\Gamma\gamma} = K^j_{\Gamma\gamma} - K^j_{\Gamma v}\ {K^j_{vv}}^{-1} K^j_{v\gamma}$$

$$\hat{K}^j_{\Gamma\Gamma} = K^j_{\Gamma\Gamma} - K^j_{\Gamma v}\ {K^j_{vv}}^{-1} K^j_{v\Gamma}$$

$$\hat{F}_\gamma = F_\gamma - \sum_j K^j_{\gamma v} \; {K^j_{vv}}^{-1} F^j_v$$

$$\hat{F}_\Gamma = F_\Gamma - \sum_j K^j_{\Gamma v} \; {K^j_{vv}}^{-1} F^j_v$$

System (8) represents the system where each zone is condensed on its border. For simplification, these notations are used: $\hat{K}^E_{\gamma\gamma} = \sum_j \hat{K}^j_{\gamma\gamma}$; $\hat{K}^E_{\gamma\Gamma} = \sum_j \hat{K}^j_{\gamma\Gamma}$; $\hat{K}^E_{\Gamma\gamma} = \sum_j \hat{K}^j_{\Gamma\gamma}$; $\hat{K}^E_{\Gamma\Gamma} = \sum_j \hat{K}^j_{\Gamma\Gamma}$. Now the second condensation on the border of the DI Γ is applied. For this, U_γ is expressed in terms of U_Γ as follow:

$$U_\gamma = {\hat{K}^E_{\gamma\gamma}}^{-1} \left(\hat{F}_\gamma - \hat{K}^E_{\gamma\Gamma} \, U_\Gamma \right) \tag{9}$$

By using this relation, system (8) is re-written as:

$$\begin{cases} \begin{pmatrix} \widehat{\widehat{K^E_{\Gamma\Gamma}}} + K^I_{\Gamma\Gamma} & K^I_{\Gamma v} \\ K^I_{v\Gamma} & K^I_{vv} \end{pmatrix} \begin{pmatrix} U_\Gamma \\ U^I_v \end{pmatrix} = \begin{pmatrix} \hat{\hat{F}}_\Gamma \\ F^I_v \end{pmatrix} & \text{(10a)} \\ U_\gamma = {\hat{K}^E_{\gamma\gamma}}^{-1} \left(\hat{F}_\gamma - \hat{K}^E_{\gamma\Gamma} \, U_\Gamma \right) & \text{(10b)} \\ U^j_v = {K^j_{vv}}^{-1} \left(F^j_v - K^j_{v\gamma} \, U_\gamma - K^j_{v\Gamma} \, U_\Gamma \right) \qquad \forall j & \text{(10c)} \end{cases}$$

where:

$$\begin{cases} \widehat{\widehat{K^E_{\Gamma\Gamma}}} = \hat{K}^E_{\Gamma\Gamma} - \hat{K}^E_{\Gamma\gamma} {\hat{K}^E_{\gamma\gamma}}^{-1} \hat{K}^E_{\gamma\Gamma} \\ \hat{\hat{F}}_\Gamma = \hat{F}^E_\Gamma - \hat{K}^E_{\Gamma\gamma} {\hat{K}^E_{\gamma\gamma}}^{-1} \hat{F}_\gamma \end{cases}$$

the resolution of (10) then proceeds with the following steps:

(a) calculation of $\hat{K}^j_{\gamma\gamma}$, the stiffness matrix of a condensed zone on its boundary, for each zone j "first condensation";
(b) calculation of $\widehat{\widehat{K^E_{\Gamma\Gamma}}}$, the stiffness matrix of the borders of the zones building the elastic domain condensed on the border of the DI "second condensation";
(c) assembly and resolution of Equation (a) of system (10) which allows to obtain U^I_v and U_Γ which are the solution on the DI;
(d) calculation, if necessary, of the displacement field at the borders of the elastic zones using Equation (10b) "level 2 decondensation";
(e) calculation, if necessary, of the displacement field inside all the condensed zones, using Equation (c) of system (10) "level 1 decondensation". This allows to reconstruct the solution on the entire structure.

Contrary to system (5) (one level condensation), a change in the elastic domain leads to recalculate ${\hat{K}^E_{\gamma\gamma}}^{-1}$ and not ${K^E_{vv}}^{-1}$. The size of the matrix to be inversed thus passes from the number of dof of the entire elastic domain to only the number of dof of the borders of the zones building the elastic domain. It is noted that with the ASC method, only Equation (10a) is solved at each time step (reduced system shown in Figure 1c). This system is reduced to only the dof of the DI and, therefore, is faster to calculate. Steps (d) and (e) are not performed at each time step but periodically, every p calculation steps. This will be detailed in the next paragraph.

Implementation of the ASC Method including Mesh Refinement of the DI

The implementation of the ASC method with mesh refinement, in the finite element code Cast3M [20], is presented in this section. The detailed implementation of the novel ASC method is found in [21]. The algorithm of the ASC method, including mesh refinement of the DI, is presented in Figure 2. For clarity, the steps of the method are illustrated on the 3-point bending beam shown in Figure 3.

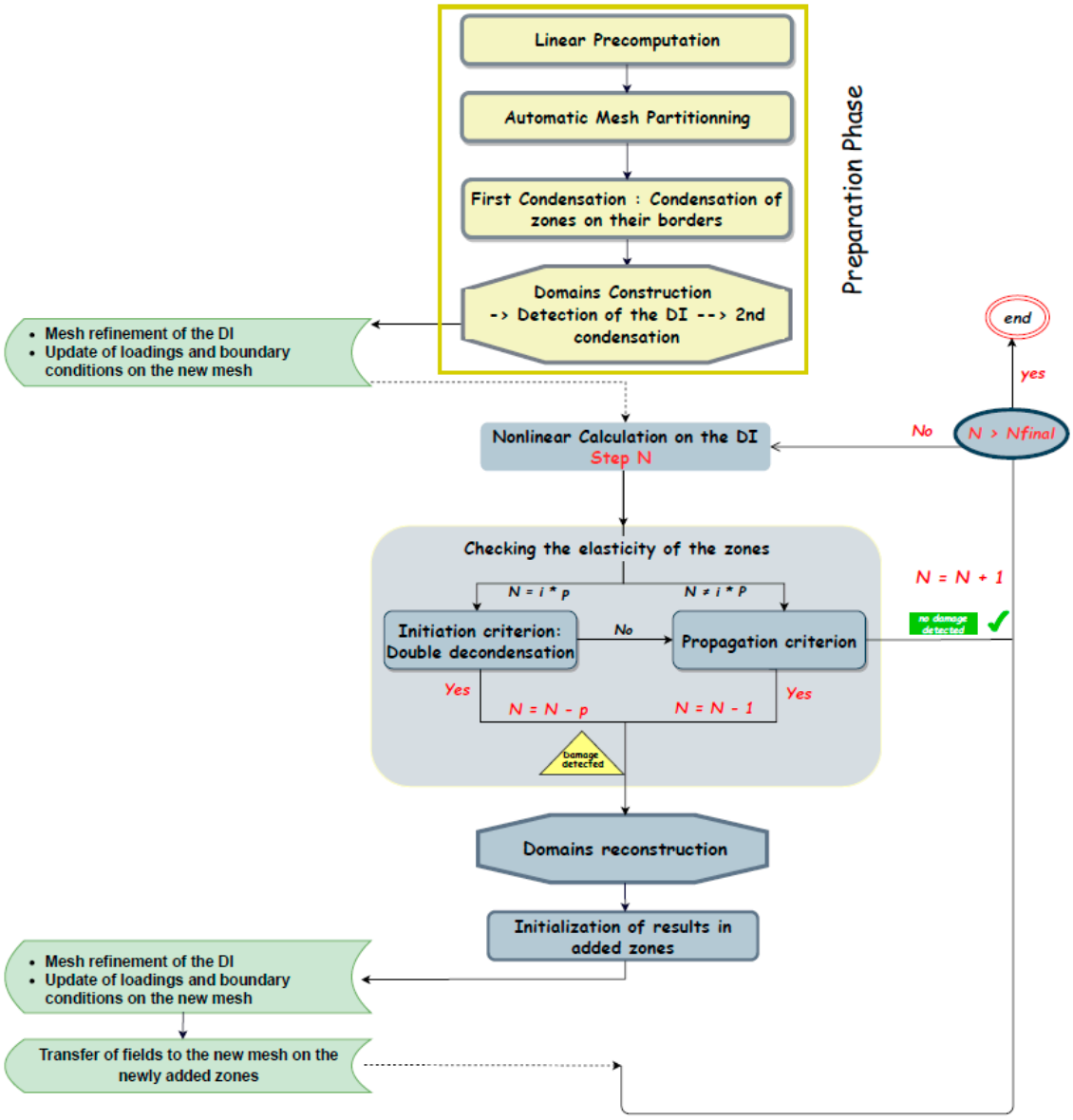

Figure 2. Algorithm of the ASC with mesh refinement (in yellow: the preparation phase, in grey: the nonlinear calculation steps, in green: the steps necessary for introducing the mesh refinement in the ASC method).

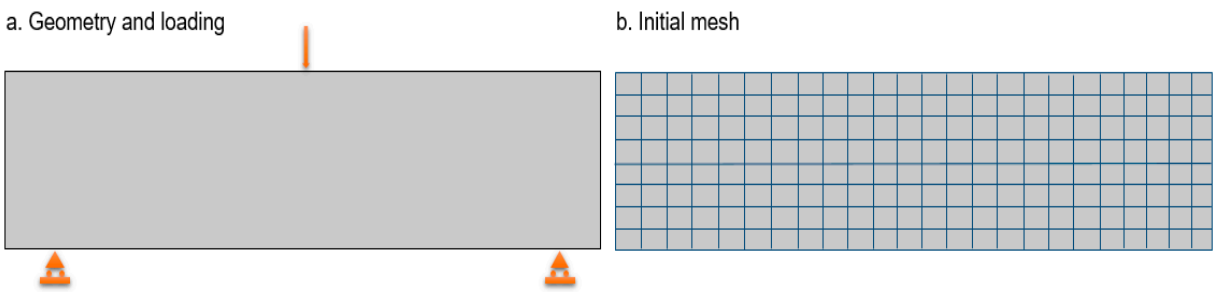

Figure 3. The simple bending beam.

2.2. Preparation Phase

Step 1. Linear precomputation

The first step consists of performing a linear precomputation on the whole structure. A distribution of the elastic deformation is obtained. When dealing with damage in concrete, the equivalent Mazars deformation ε_{eq}, is then calculated using the following equation [22] (Figure 4a):

$$\varepsilon_{eq} = \sqrt{\langle \varepsilon_1 \rangle_+^2 + \langle \varepsilon_2 \rangle_+^2 + \langle \varepsilon_3 \rangle_+^2} \tag{11}$$

where $\langle \varepsilon_i \rangle_+$ represents the principal positive values of the strain.

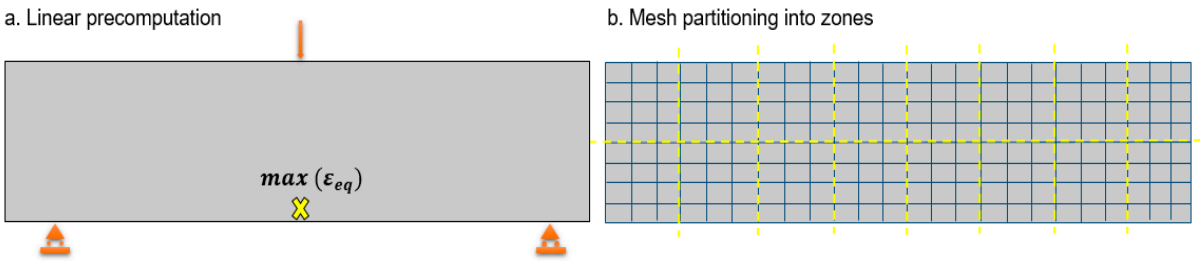

Figure 4. Linear precomputation and mesh partitioning on the simple bending beam.

Step 2. Automatic mesh partitioning

The elastic distribution of ε_{eq} is used to partition the total mesh into zones (Figure 4b). This partitioning is carried out using an automatic partitioning procedure adapted to the ASC method developed in [19]. It is based on the physical interpretation of damage initiation and propagation. In Figure 4b, for sake of illustration, the mesh is partitioned into 16 zones of equivalent sizes.

Step 3. First Condensation

This step consists of replacing the stiffness and the loadings inside each zone by boundary conditions on its borders (Figure 5). This is carried out using Guyan's static condensation, as presented in Section 2.1. It should be noted that as the partitioning of mesh into zones is carried out in the preparation phase and does not evolve during computation, this calculation step is only carried out once.

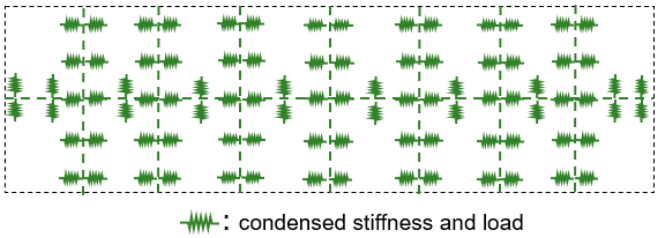

Figure 5. First condensation on the simple bending beam.

Step 4. Domain construction

This step allows to build the first DI, which is to be activated and fully modeled. The elastic domain is condensed and replaced by boundary conditions on the border of the DI. The initial DI is built from the most damageable areas, i.e., the areas that include the elements with the maximum of ε_{eq}. A second condensation is then performed. Using Guyan's static condensation, the second condensation (Figure 6b) calculates the boundary conditions on the border of the DI, from the results of the first condensation as presented in Section 2.1.

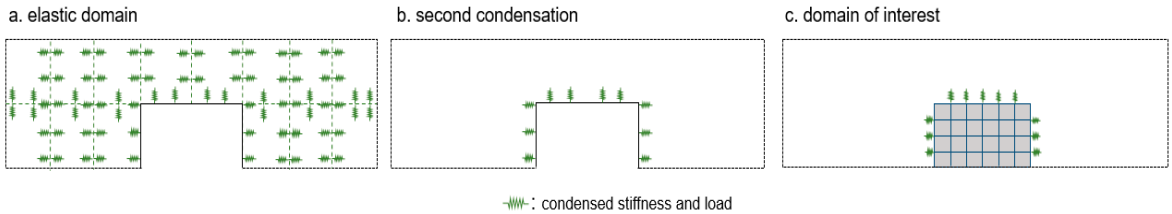

Figure 6. Construction of domains on the simple bending beam.

Step 5. Mesh refinement inside the DI

The objective of this step is to select an appropriate level of refinement for the target mesh based on the user's specified precision criterion. This criterion should enable an accurate simulation of the behavior of the modeled materials. For example, this could entail using a mesh that facilitates the use of a regularization technique to address mesh dependency issues. In the case of employing a non-local model to simulate concrete [23], this might be related to the size of the largest aggregate in the concrete. If the initial mesh does not meet the required level of refinement, it is considered "coarse", and a mesh refinement process is initiated to achieve the desired target refinement. There are two primary approaches to achieving this, including re-meshing techniques and refinement techniques. Re-meshing involves completely rebuilding the mesh with the target refinement [24–26] or adapting the mesh by relocating its nodes based on an error map of the initial mesh [27,28]. The second solution utilizes the elements of the initial mesh to generate a new, finer one by locally enriching the spatial discretization [29]. Our study employs this second technique, as it is easier to implement and facilitates field transfer from the coarse mesh to the fine one. To maintain the performance associated with double condensation, the discretization of the DI boundary remains the same, and refinement is only performed within the DI. We select an "h-refinement" approach [30], which modifies the element size to achieve smaller elements, as opposed to the less suitable "p-refinement" technique that employs higher-order shape functions. This hierarchical approach is straightforward to implement, and the final mesh is obtained by subdividing the elements of the initial mesh until achieving the desired level of refinement. Figure 7 offers an illustration of the initial and refined meshes.

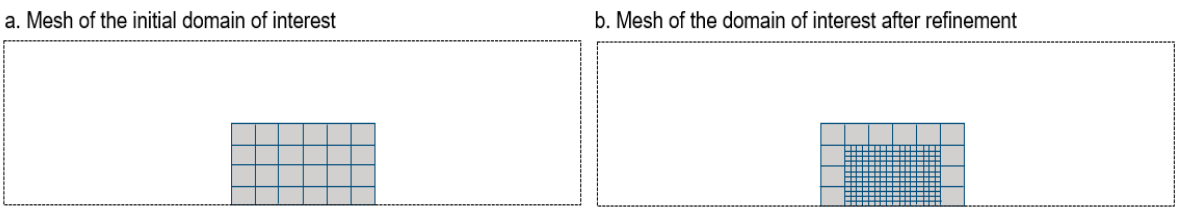

Figure 7. Mesh refinement of the DI.

It is important to acknowledge that the refinement process generates "hanging nodes", which create non-conformities where certain nodes at the interface between fine and coarse elements do not coincide. Figure 8 presents an example of this phenomenon in a simplified configuration. To ensure the continuity of displacement at each "hanging node" n_i located at the interface $\mathrm{I}_{G,F}$ between a coarse element E_G and its corresponding fine elements E_F, kinematic relations are employed. These relations utilize the shape functions (N_j^G) of the coarse element [29]:

$$u_i = \sum_{x_j \in E_C \cap \mathrm{I}_{C,F}} N_j^C(x_i) u_j \tag{12}$$

which, for example, gives for the hanging point of Figure 8a the following conformity relation:

$$U_C = \frac{1}{2}(U_A + U_B) \tag{13}$$

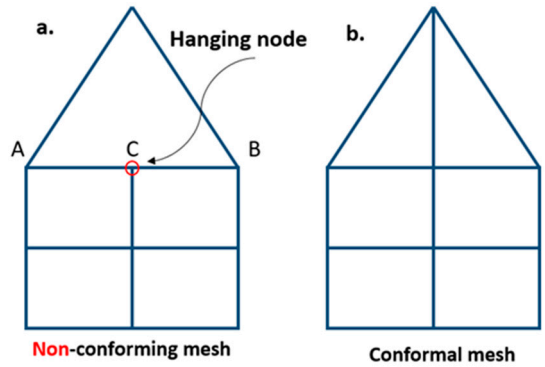

Figure 8. Difference between conformal (**b**) and non-conforming mesh (**a**).

These relations are imposed via Lagrange multipliers in the same way as the Dirichlet boundary conditions [31]. It should be noted that other solutions may have been possible such as the creation of new elements (Figure 8b).

Finally, after refinement, the loadings and boundary conditions are updated on the new mesh if necessary. For example, the self-weight, distributed on all the nodes of the structure, is redistributed on the new nodes after refinement.

2.3. Nonlinear Calculation Steps

The nonlinear calculation is carried out on the DI only by using the stiffness of the condensed zones as additional boundary conditions. This calculation is equivalent to the calculation without condensation, as long as the condensed domain remains elastic. This is verified using a propagation criterion and a priming criterion. The propagation criterion evaluates the potential propagation of damage from the existing DI to the neighboring condensed zones. Propagation bands are defined over a width L from the border of the DI (in orange in Figure 9a). This parameter does not affect the accuracy of the calculation but has a significant impact on the performance of the ASC method. Indeed, a large value of L triggers the early activation of neighboring zones, which may not be damaged at the end of the calculation, thereby penalizing the performance. Therefore, a study was conducted in [21] and showed that to optimize the method's performance, this parameter should be set equal to the characteristic length L_C in the case of a non-local calculation and to a single row of elements on the boundary of the DI in the case of a local calculation. If damage reaches these bands, the neighboring area is promoted as a new interest zone and is added to the DI. This criterion is checked at the end of each calculation step, as the cost of this verification is negligible. In the case of propagation, as shown in Figure 9b, the current step is recalculated, using the new refined DI, in order to avoid any miscalculation. It is noted that using this criterion, the border elements of the DI never include any damage.

The second criterion is related to the initiation of new damaged zones, independently of the existing DI. A "decondensation" (Equations (b) and (c) of system (10)) is thus carried out periodically to obtain the values of the displacements on the entire structure. If a defined "limit of elasticity" is exceeded in a given zone, it is then included in the new DI. As decondensation requires the calculation of the inverse of a large matrix and can therefore be expensive, this criterion is checked only after each p steps of loading (p generally fixed to 8 as a result of a sensitivity analysis carried out in [19]). Once again, to avoid any miscalculation, if a new zone appears, the p last loading steps are recalculated. It is to be noted that the verification of this criterion, which is one of the most expensive steps of the method, is performed on the initial mesh of the condensed zones (without any refinement).

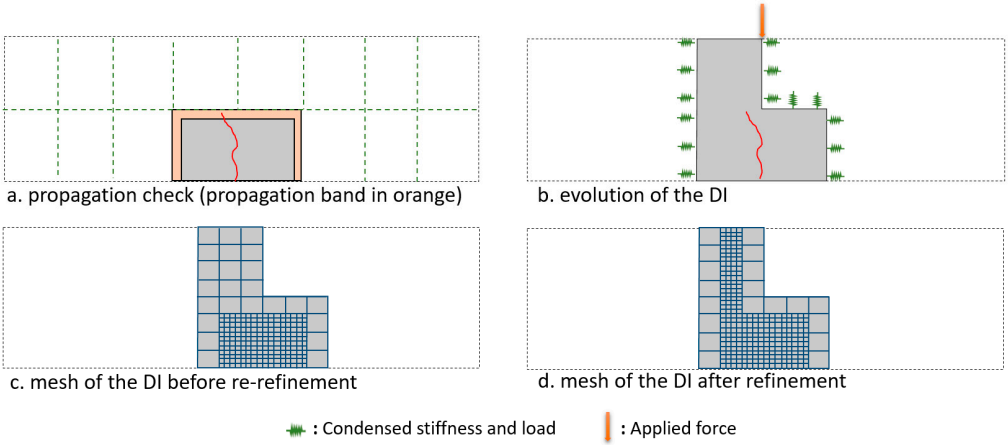

Figure 9. Propagation criterion.

In both cases (propagation and initiation), when the DI evolves, a domain reconstruction is performed, taking advantage of the two-level condensation and using the "second condensation" only. The mesh of the new DI is refined in the same way as in step 5 (see Figure 9d), and the boundary conditions and loadings are updated on this new refined mesh, if necessary.

The refinement of the new DI, which is performed during the calculation, requires that the fields of displacement, internal variables, deformations, and stresses are updated on the new mesh. The updated fields include nodal fields (e.g., the displacement field) and fields at the Gaussian points (stress, internal variables, . . .). In addition to the traditional "decondensation" of these fields on the initial mesh, an additional step is necessary here to transfer the fields of the initial mesh onto the refined one. Several methods exist in the literature to achieve this transfer, such as the minimization method [32] or the interpolation method [33].

For the nodal fields, the method of interpolation using the shape functions of the initial mesh is chosen. This method is detailed in [32]. For a given node of the refined mesh, the element of the initial mesh in which it is included is found. Then, using the shape function of the element and the position of the node, the field value is interpolated.

To transfer the fields defined at Gaussian points ($\underline{x}$), the difficulty lies in the fact that only values at discrete points are available. There is no continuous approximation of the field over the entire domain. To project the fields from the initial mesh Ω^n towards the refined one Ω^{n+1}, the method from [32] is used. To transfer the field F^n defined at the Gauss points of Ω^n, the first step consists of transforming it into a nodal field $\overset{\sim n}{F}$ using the shape functions N^n associated with the elements of Ω^n (Figure 10b). This is carried out by solving the following equation:

$$\int_{\Omega^n} N^n(\underline{x}).N^{n\,T}(\underline{x}).\overset{\sim n}{F}\, d\Omega = \int_{\Omega^n} N^n(\underline{x}).F^n(\underline{x}) d\Omega \tag{14}$$

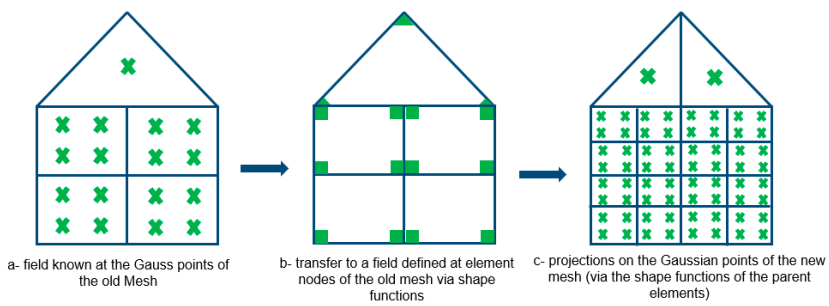

Figure 10. Illustration of the transfer of a field defined at the Gauss points.

The second step consists in finding for each Gauss point $\underline{x}_i^{n+1}$ of Ω^{n+1}, the element of Ω^n in which it is located and to calculate its local coordinates. The calculated nodal field $\underset{\sim}{F}^n$ is interpolated on the new mesh like the other nodal fields (Figure 10c) and gives the final field F^{n+1} as follows:

$$F^{n+1}\left(\underline{x}_i^{n+1}\right) = N^{nT}\left(\underline{x}_i^{n+1}\right).\underset{\sim}{F}^n \tag{15}$$

This method is illustrated in Figure 10. As explained, a uniform refinement of the interior mesh of the DI is carried out here, not an adaptive mesh refinement (AMR), which evolves in space and time. The mesh of a zone, once refined, no longer evolves. If an AMR was applied in the DI, the mesh of an element with nonlinear behavior could evolve and require the transfer of fields from its old mesh to the new one. This transfer would require more complex transfer methods and could induce inaccuracies in the results. In the ASC method, these transfers are only necessary in the new zones of the DI, which by definition have an elastic behavior at the time of transfer. Thus, the risk of inaccuracies related to the projection is limited. For example, damage is never concerned with the projection (as, at the moment of refinement, the concerned zones have uniformly null damage). This is one of the reasons why a simple mesh refinement of the DI is applied in this contribution.

2.4. Validation on a 2D Notched Bending Beam

To test the applicability of the ASC method with mesh refinement, a notched bending beam is considered. The beam is 160 cm long and 40 cm high. It is modeled in 2D (plane stress hypothesis) with an equivalent thickness of 20 cm. The beam is notched at mid-length. The notch is 80 mm high and 8 mm wide. The initial mesh shown in Figure 11a is composed of 610 quadrilateral elements of 4 cm side length each. Concrete is modeled using Mazars' damage model [22] with the parameters given in Table 1. These parameters allow a compressive strength of 41.4 MPa and a tensile strength of 3 MPa. The Mazars model is an isotropic damage model that assesses the material response using a scalar damage criterion "D" based on deformations. It was developed within the framework of damage mechanics and is commonly used to model concrete as it accurately reproduces its behavior. The stiffness reduction resulting from the creation of microcracks in concrete is described as follows:

$$\sigma = (1 - D)E : \varepsilon^e \tag{16}$$

where E is the Hooke's matrix and ε^e is the elastic strain. The damage variable D ranges from 0 (undamaged material) to 1 (completely damaged material). To calculate this variable, Mazars introduces the concept of equivalent strain ε_{eq}, calculated using Equation (11), which translates the triaxial state into equivalent uniaxial states. D is defined as a combination of tensile damage D_T and compressive damage D_C as follows:

$$D = \alpha_T^\beta \ D_T + \alpha_C^\beta D_C \tag{17}$$

D_t and D_C are expressed as follows:

$$\begin{cases} D_T = 1 - \frac{(1-A_t)\varepsilon_{d_0}}{\varepsilon_{eq}} - A_t \ \exp\left(-B_t\left(\varepsilon_{eq} - \varepsilon_{d0}\right)\right) \\ D_C = 1 - \frac{(1-A_c)\varepsilon_{d_0}}{\varepsilon_{eq}} - A_c \ \exp\left(-B_c\left(\varepsilon_{eq} - \varepsilon_{d0}\right)\right) \end{cases} \tag{18}$$

where A_t, A_c B_t, and B_c are material parameters. β is a coefficient introduced to enhance shear behavior and its value is set to 1.06. The coefficients α_T^β and α_C^β establish a relationship between damage and the state of compression or tension:

$$\begin{cases} \alpha_T^\beta = \left(\sum_{i=1}^{3} \frac{<\varepsilon_i^t><\varepsilon_i>_+}{\left(\varepsilon_{eq}\right)^2}\right)^\beta \\ \alpha_C^\beta = 1 - \alpha_T^\beta \end{cases} \tag{19}$$

where $< \varepsilon_i^t >$ is the principal positive strain value and $< \varepsilon_i >_+$ is the positive principal strain value. Physically, due to the heterogeneity of the concrete microstructure, there exists an interaction between cracks formed at a given distance. Therefore, the stress state at a given point must account for its surroundings. This consideration is not addressed in a local model and results in a solution dependent on meshing. To mitigate this mesh dependence, non-local regularization methods exist [34,35]. The method utilized in this application is the averaging (integral) method [23], which involves averaging the local equivalent strain ε_{eq} over a defined volume V using a parameter known as the characteristic length L_C. It is worth noting that the ASC method is adaptable to any other type of damage and/or plasticity models that simulate the behavior of reinforced concrete structures.

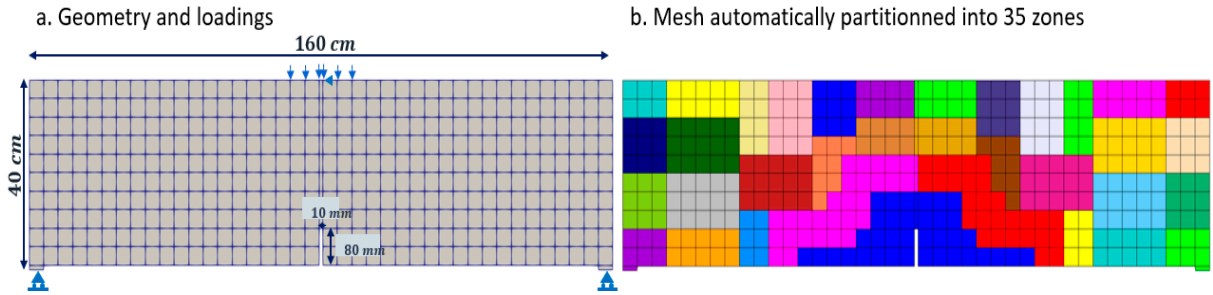

Figure 11. Notched bending beam.

Table 1. Mazars Parameters—notched bending beam.

Young's Modulus (E)	Poisson Coefficient (ν)	Elastic Limit (ε_0)	Parameter 1 Compression (A_C)	Parameter 2 Compression (B_C)	Parameter 1 Traction (A_T)	Parameter 2 Traction (B_T)
30 GPa	0.24	4×10^{-5}	1.25	1000	0.90	4×10^3

A downward imposed vertical displacement of up to 200 µm is applied over a length of 8 cm at the top of the beam. Vertical movement is blocked at the support points and horizontal movement is blocked at the upper midpoint. The structure is initially partitioned into 35 zones, as shown in Figure 11b, using the automatic mesh partitioning procedure. This method is based on physical considerations, taking into account the anticipated shape and evolution of the damaged regions during loading. (A comprehensive explanation of this partitioning method is available in [19]). In the DI, a refinement of 1 cm is targeted. This size allows to avoid any mesh dependency of the results by applying a non-local integral method [23] with a characteristic length $L_C = 3$ cm. All calculations are carried out on the same 24-core computing node in order to be able to compare calculation times with identical hardware.

The ASC calculation results are presented in Figure 12. This figure shows the evolution of the damage and the DI during the loading. Damage initiates around the notch, then propagates. It also appears at the support zones. The figures especially illustrate the progressive refinement of the mesh with the propagation of the damage. The comparison with a complete computation using a fine mesh (1 cm throughout the structure) is then proposed. Figure 13 presents the distribution of the damage at the end of the complete computation. This profile and that resulting from the ASC calculation with mesh refinement given in Figure 12, are identical where they can be compared (in the DI when using ASC).

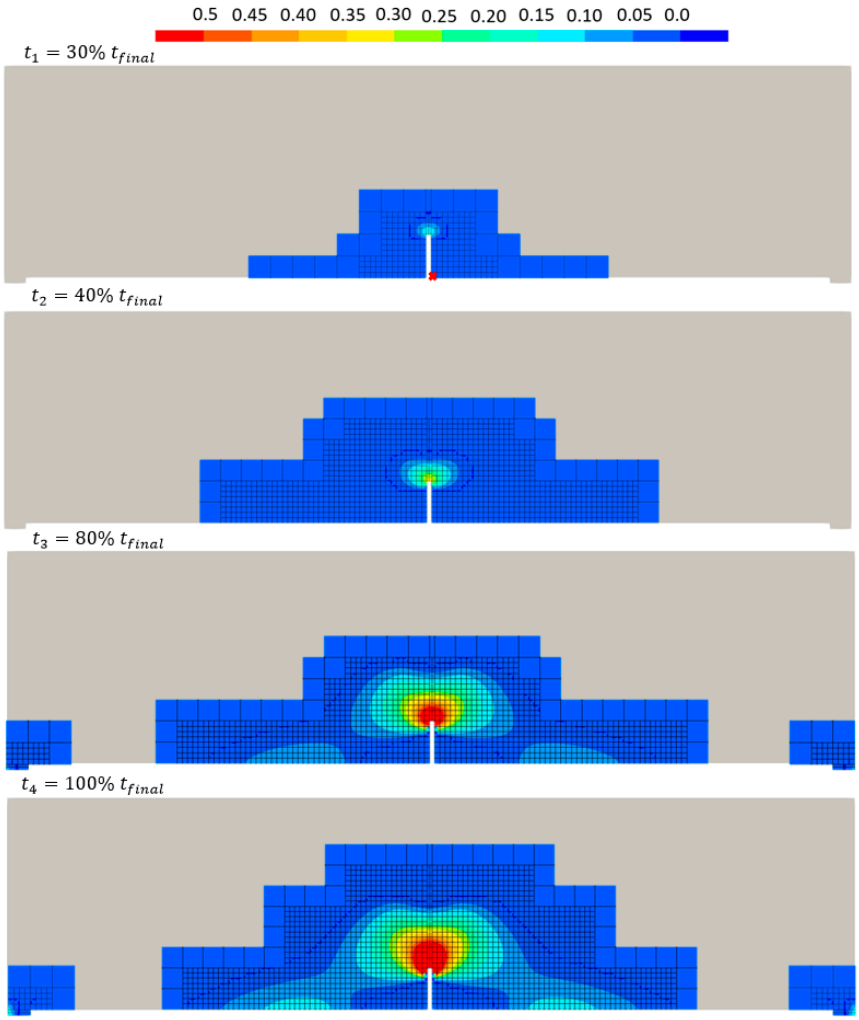

Figure 12. Evolution of the DI and the damage obtained with the ASC/MR (the red point in the first figure will be post-processed later).

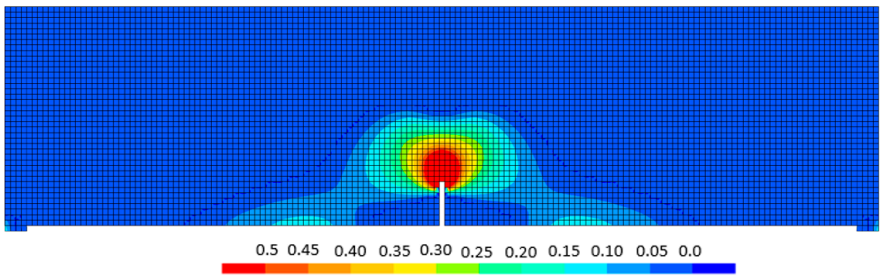

Figure 13. Damage profiles at the end of the complete simulation.

A third calculation with the ASC method is carried out, but with an initial uniform mesh size of 1 cm over the entire structure (without mesh refinement). Figure 14 presents the evolution of the notch opening and of the vertical displacement at a median low point (red point in Figure 12) of the beam for the three calculations. A perfect correspondence between the results of the complete calculation and the ASC calculation without refinement is shown in this figure, as are the very close results for the ASC calculation with refinement. This slight difference is due to the slight difference in refinement of the mesh compared to the mesh of the complete calculation (see meshes above the notch in the two calculations). The calculations are compared in terms of performance in Table 2. The gain factor is calculated in the following table and throughout the remainder of the article as the ratio

between the computation time of the complete calculation (without using condensation) and the time required to perform the same calculation on the same machine, but using the ASC method. These results show an improvement in the gain factor from 6.2 to 9.6 when using the ASC method with the DI mesh refinement.

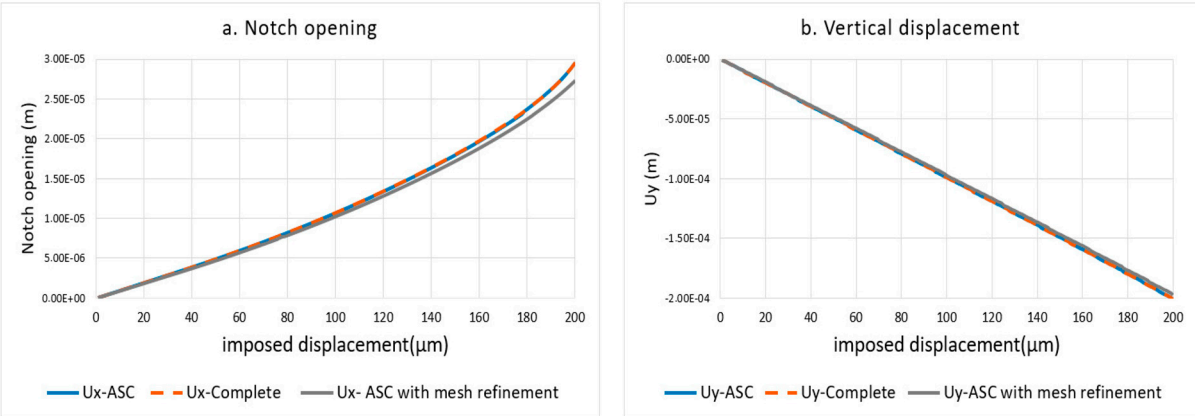

Figure 14. Evolution of displacements in the two directions in terms of loading.

Table 2. Numerical efficiency results.

	Complete Calculation	ASC Calculation (1 cm)	ASC/MR (4 cm–1 cm)
Calculation time	550 s	88 s	58 s
Gain Factor	1	6.2	9.6

2.5. Simplified Containment Vessel under Pressure (Reinforced Concrete Structure)

After validation of the proposed approach on a simple application, a more representative test case is now studied to go further in the analysis in terms of computational efficiency and numerical "representativeness". This test case is a reinforced concrete cylinder with a hemispherical dome. The structure is loaded with an internal pressure. It is chosen to be as close as possible to a scaled representation of a nuclear containment vessel [36]. It is 3.5 m high and 5 cm thick, with an external radius of 1.75 m. It includes a rectangular opening of 60 × 40 cm section. The structure includes 60 hoops and 20 vertical bars in the wall and 20 U-shaped bars passing through the wall and the dome (Figure 15b). "Perfect" kinematic relations ensure the same displacements between steel and concrete. Mazars's damage law is used for concrete with the parameters from [18]. A linear elastic law is chosen for reinforcement ($E = 200$ GPa ; $\nu = 0.2$). The displacements at the bottom of the structure are blocked, and the structure is loaded with an increasing internal pressure up to 1 bar. For simplicity reasons, the internal pressure is applied to the internal surface of the structure (open) and without special treatment to replace the window.

It is to be noted that the presence of the steel reinforcement requires particular care for refinement. It is customary to include at least one steel node inside each concrete element through which the reinforcement passes. This therefore assumes that the steel elements are also refined during the refinement of the concrete elements, until each concrete element contains at least one steel node.

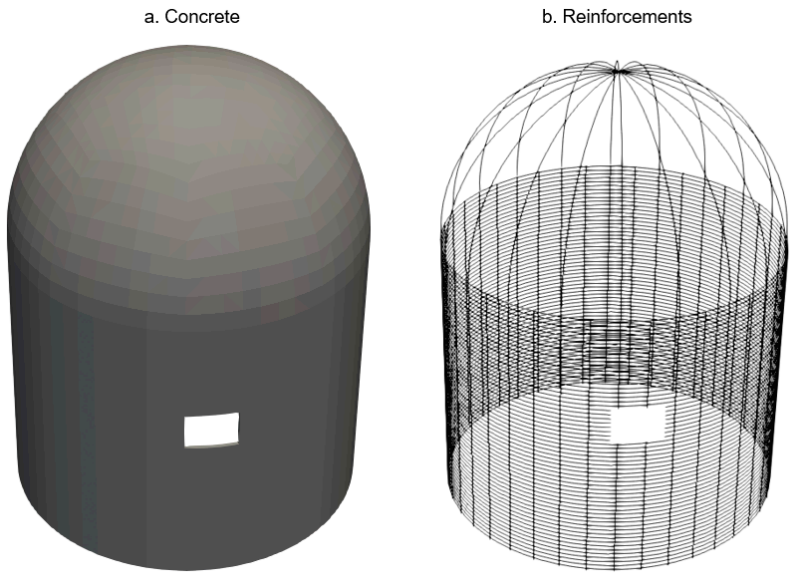

Figure 15. Simplified containment vessel.

Figure 16 gives an illustration before and after the refinement. This step also supposes to update the kinematic relations, including the new steel and concrete nodes.

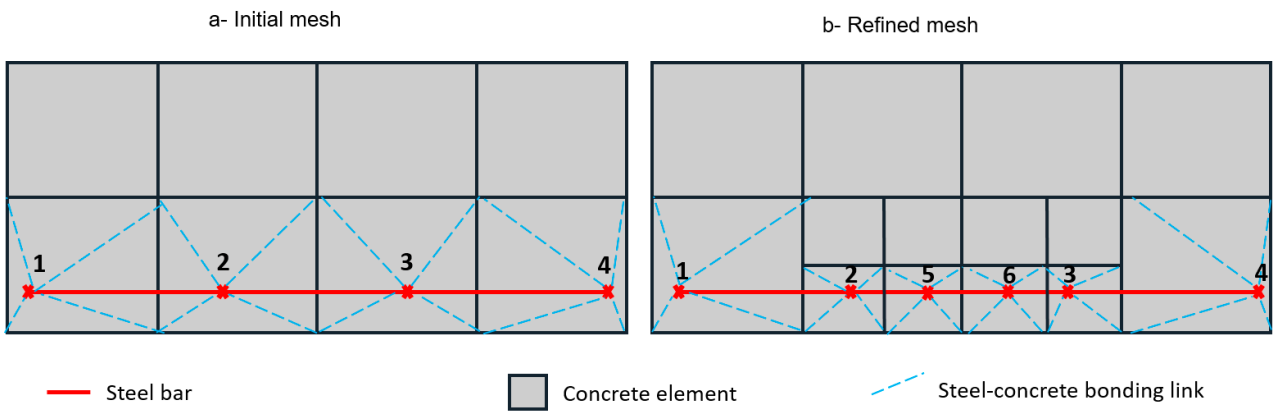

Figure 16. Mesh refinement of a reinforced concrete beam.

The concrete is meshed with linear hexahedral finite elements (8 nodes), and the reinforcements are modeled with linear bar elements with 2 nodes (diameter $\phi = 3.2$ cm). In order to quantify the effect of mesh refinement, different meshes are used (see Figure 17): From the coarse mesh (1722 hexahedrons of 20 cm side length with only 1 element in the thickness) to the extra-fine mesh (1,721,600 elements of 1.25 cm side length with 16 elements in the thickness). The extra-fine mesh allows for the application of a regularized damage model for concrete. Four comparisons are made for 4 mesh sizes between a complete calculation and an ASC calculation, starting from the coarse mesh and refining the DI until reaching the refinement of the complete calculation. Note that with the hierarchical refinement used, the refinement obtained is close (lower) but not exactly the same as the complete mesh. With a local damage model, this may induce a slight difference in the results. The first three tests use a local damage model, whereas the fourth uses a non-local integral model as the element size is fine enough. The details of the four tests are summarized in Table 3. All computations are performed on a 24-core/128 GB RAM computing node. Figure 18 shows the mesh partitioning used for ASC calculations. This mesh is obtained using the automatic partitioning method developed in [37]. This partitioning is performed on the coarse mesh, and it is the same for all ASC calculations because the preparation phase is always performed on the initial mesh, which is the coarse one for the ASC calculations.

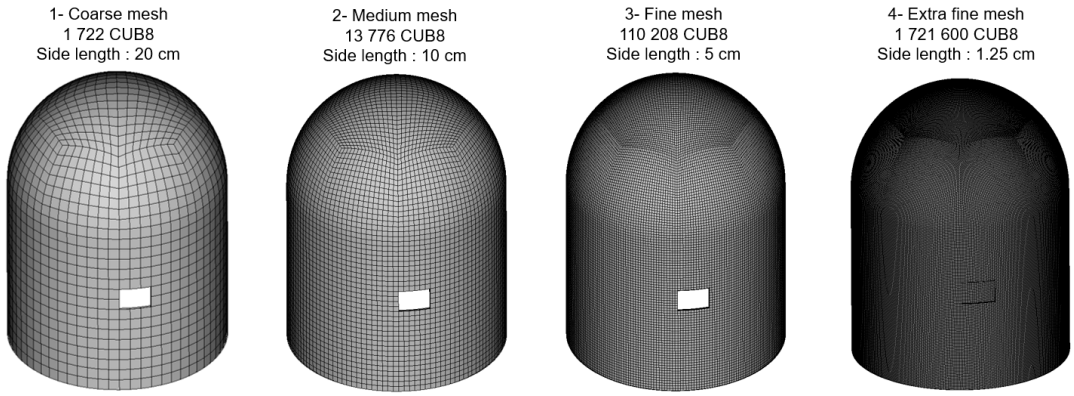

Figure 17. The different meshes used.

Table 3. Summary of performed tests.

Number of Test	Target Mesh Density	Mesh of the Complete Calculation	Mesh of the ASC/MR Calculation	Damage Model
1	20 cm	Coarse	coarse in the ED coarse in the DI	Local
2	10 cm	Medium	coarse in the ED medium in the DI	Local
3	5 cm	Fine	coarse in the ED fine in the DI	Local
4	1.25 cm	Extra-fine	coarse in the ED extra-fine in the DI	Non-local (L_c = 4 cm)

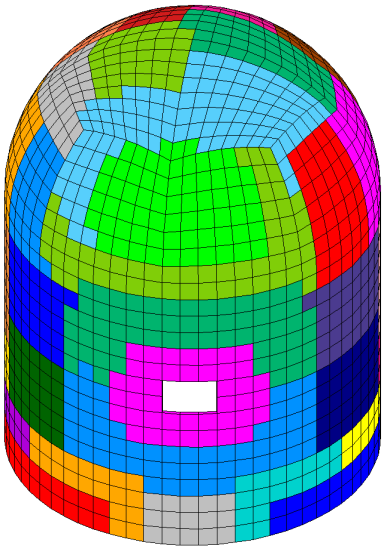

Figure 18. Mesh partitioning used for ASC calculations.

The damage for the case with an applied pressure equal to 1 bar for the first test is presented in Figure 19. At the end of the calculation, the damage is concentrated around the opening in a relatively limited area. It results in the activation of the zone surrounding the opening with the ASC method. The same damage distribution is obtained in both calculations. The results of the computational performance are presented in Table 4 and show a time saving of a factor of 5.3 by using the ASC method with respect to the complete calculation.

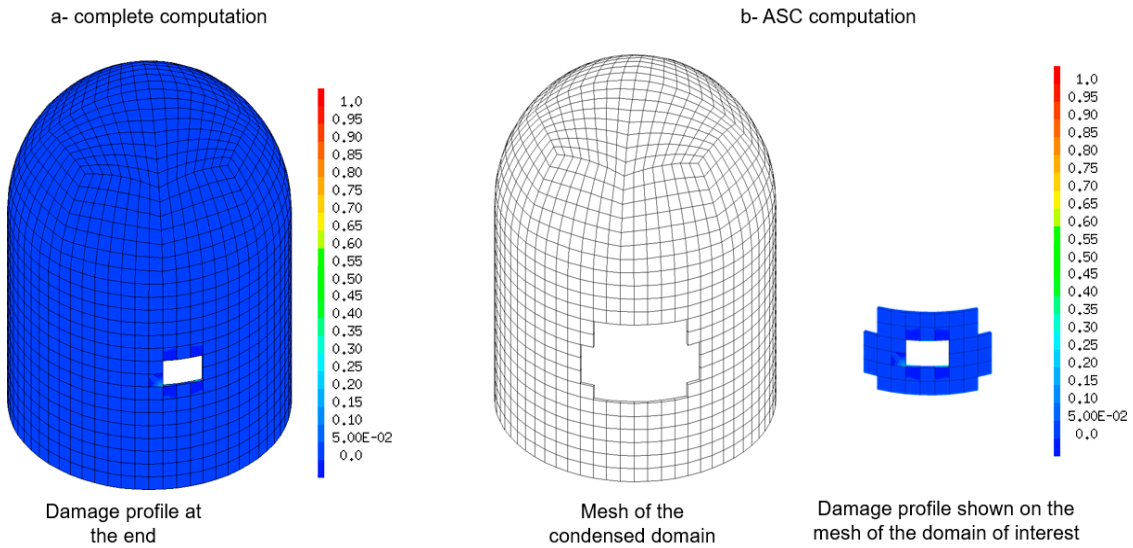

Figure 19. Calculation results—coarse mesh (20 cm).

Table 4. Computational performance results—1st test.

	Complete Calculation	ASC Calculation
Degrees of freedom	39,516	1776
Calculation Time	96 s	18
Gain factor	1	5.3

Figure 20 shows the damage at the end of the calculation at a 1 bar pressure during the second test using the medium mesh. The distributions of damage resulting from the complete calculation and from the ASC calculation with mesh refinement are very close. Compared to the results obtained on the coarse mesh, the mechanical degradation is more pronounced here. This resulted in the activation of the propagation zones surrounding the initial DI. With regards to the computational performance presented in Table 5, the ASC calculation with mesh refinement is about 13 times faster than the complete calculation.

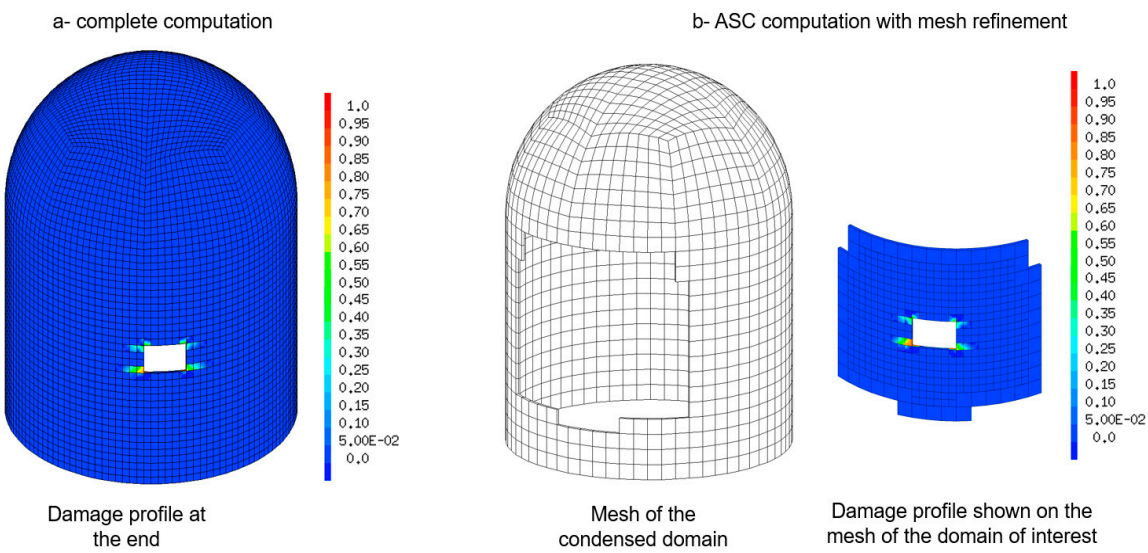

Figure 20. Calculation results—Medium mesh (10 cm).

Table 5. Computational performance results—2nd test.

	Complete Calculation	ASC/MR Calculation
Degrees of freedom	120,780	13,206
Calculation time	546 s	40 s
Gain factor	1	13.6

The damage at 1 bar pressure in the third configuration is shown in Figure 21. It propagates further, with a large damaged area around the opening. An analysis is carried out in the following Section 2.6 to include/understand the difference in damage profiles when using this finer mesh. The calculation performances presented in Table 6 indicate a gain of about 14 on the calculation time.

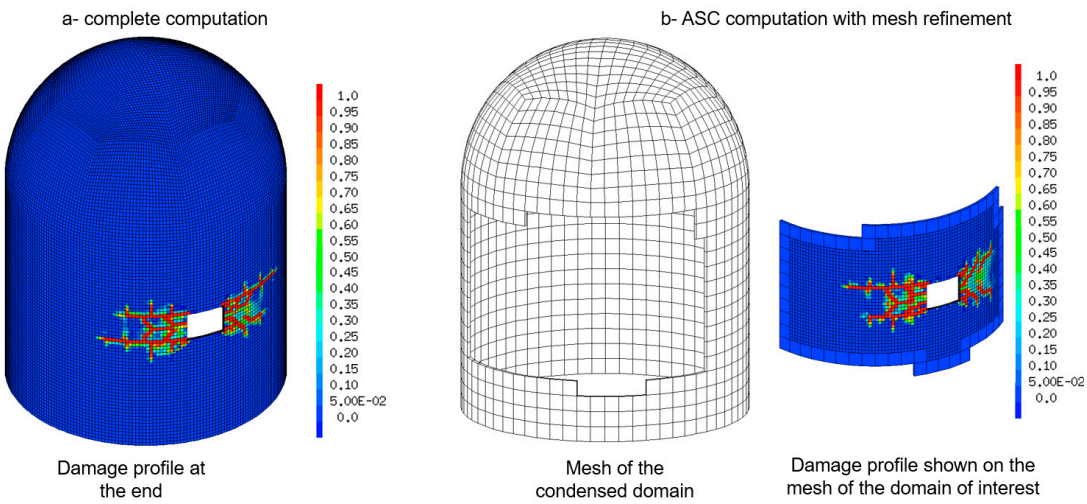

Figure 21. Calculation results—fine mesh (5 cm).

Table 6. Computational performance results—3rd test.

	Complete Calculation	ASC/MR Calculation
Degrees of freedom	533,094	63,540
Calculation time	8824 s	631 s
Gain factor	1	13.98

The 4th and last test is a calculation with a target refinement of 1.25 cm, to allow the use of a non-local damage model in the concrete. A non-local integral model [23] is chosen with a characteristic length $L_C = 4$ cm. The complete calculation using the extra-fine mesh has around 6 million degrees of freedom. The non-local damage model is costly, and it consists, for each finite element, of a search for the elements located in a neighborhood defined by the characteristic length $L_C = 4$ cm, then of an averaging of the equivalent deformation (which is then used to calculate the damage) on the found elements. Given the numerical cost of using a non-local model and the number of degrees of freedom, the complete calculation cannot be completed here because it reaches the memory limits of the calculation node. The calculation using the ASC method with mesh refinement and starting from an initial mesh of 20 cm side length can be carried out because it has 18 times fewer degrees of freedom than the complete mesh (see Table 7 for computational performance details). The evolution of the DI during the calculation and the damage distributions are presented in Figure 22. These profiles clearly show the effect of the non-local model, with damage distributed over a distance related to the characteristic length. This calculation was completed in 306,489 s (about 3.5 days). It is to be noted that the simulation using the

ASC method with an extra-fine uniform mesh (without refinement) cannot be completed for the same memory limitation as the full calculation. This demonstrates the interest in using the DI mesh refinement in the ASC method.

Table 7. Computational performance results—4th test.

	Complete Calculation	ASC/MR Calculation
Degrees of freedom	5,998,686	337,200
Calculation time	×	306,489 s

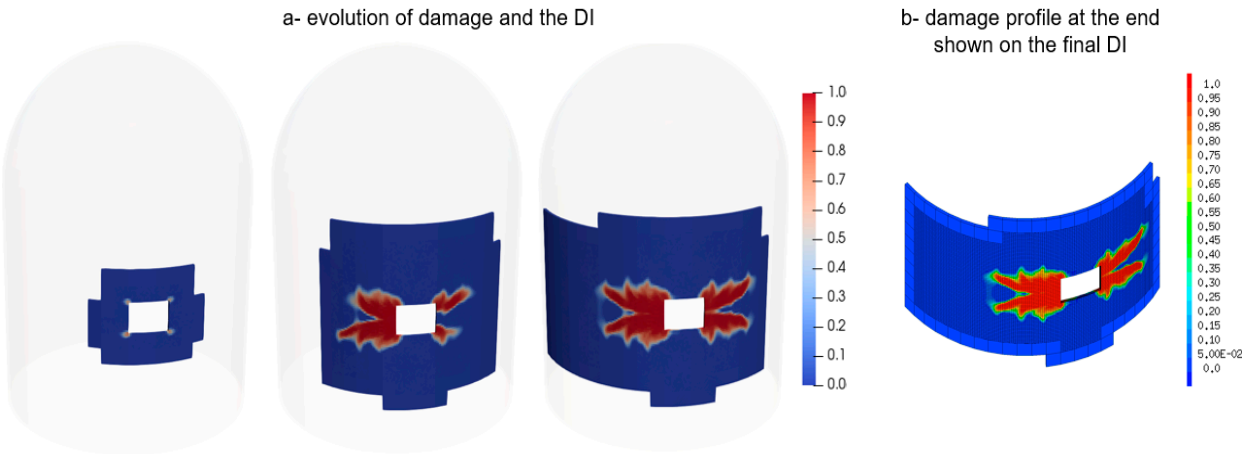

Figure 22. Damage evolution—extra-fine mesh (1.25 cm).

The radial displacement of the red point in Figure 23 is plotted against pressure to evaluate the effect of using a coarse mesh in the condensed domain. These displacements are plotted for the first three meshes (coarse, medium, and fine) and compared to the complete calculation. We note that additional post-processing (decondensation) is necessary to obtain the evolution of displacement at the identified point because it does not belong to the activated DI.

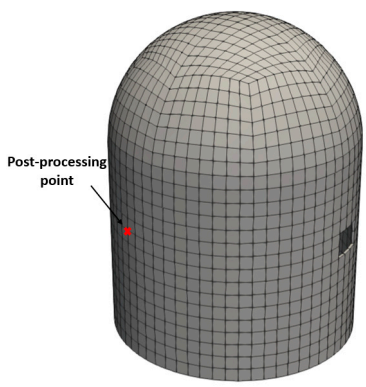

Figure 23. Post-processing point.

For the coarse and medium mesh, the complete computation and the ASC method give very close results (Figure 24a). There is almost a linear evolution between the pressure and the radial displacements. For the fine mesh (Figure 24b), a linearity is observed between the pressure and the radial displacement before a nonlinear evolution. The results between the ASC method and the complete calculation in the linear part are identical. In the nonlinear part, the results remain close. This difference is related to the slight difference in mesh density between the two calculations. These results show that the nonlinearity that is observed in the DI has a direct influence on the evolution of the displacements in the other

zones. This impact can also be captured when using the ASC method, even when using a coarse mesh in the condensed domain, because the damage in the zone of interest is correctly reproduced.

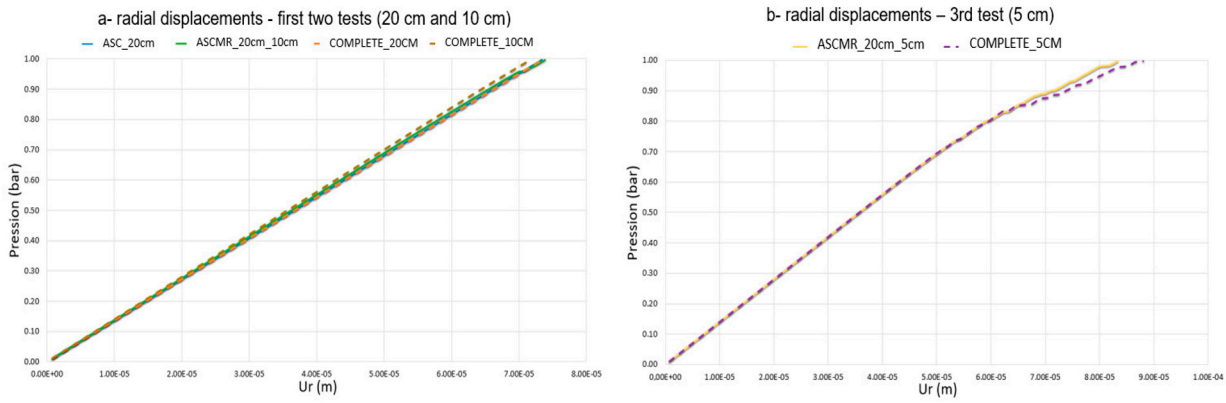

Figure 24. Comparison of the behaviors in the condensed domain.

2.6. Discussion on the Obtained Results

The previous results on the simplified containment vessel have shown damage propagation, which depends on the mesh refinement. This mesh dependency is expected to be related to local damage approaches but also to stress concentration around the openings. To go further in the analysis, the evolutions of the displacements at three particular points (Figure 25) are studied:

- P_P is a point close to the opening (a corner of the opening)
- P_M is a point moderately far from the opening (distant 1.20 m from the opening)
- P_L is a point far from the opening (about 3.6 m) and is located in a zone, which remains elastic.

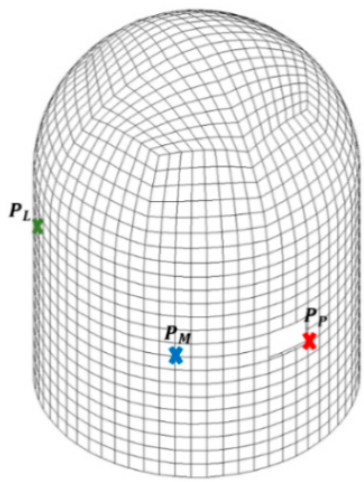

Figure 25. The 3 post-processing points.

Figure 26 provides the evolution of the radial displacements for the 3 points as a function of the pressure for the three mesh densities. The results obtained for point P_P (Figure 26a), show a great difference even in the elastic part of the curve. This difference is less significant for point P_M (Figure 26b). As for point P_L, the results with the 3 meshes are almost identical in the elastic part (see Figure 26c).

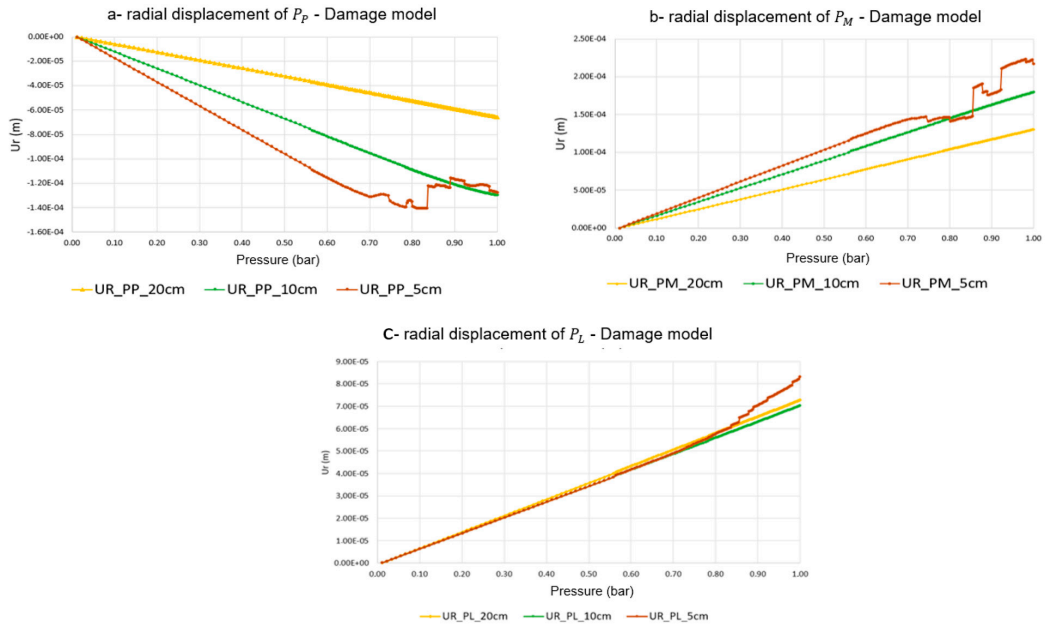

Figure 26. Radial displacements on the 3 post-processing points and for 3 mesh refinements—Mazars model for concrete.

In order to overcome the potential effect of damage, the same test is carried out using an elastic model for concrete. The results are given in Figure 27. A significant difference with the mesh density is still here at point P_P, and becomes less significant with the distance from the opening (point P_M then point P_L). It confirms the influence of both damage model and stress concentration near the opening in the mesh dependency of the results. As a final analysis, an elastic computation is performed without considering the opening (Figure 28). The evolution of the radial displacement for a given pressure (1 bar) as a function of the angular position is studied. In this case, no mesh dependency is observed, which confirms the major role of the opening.

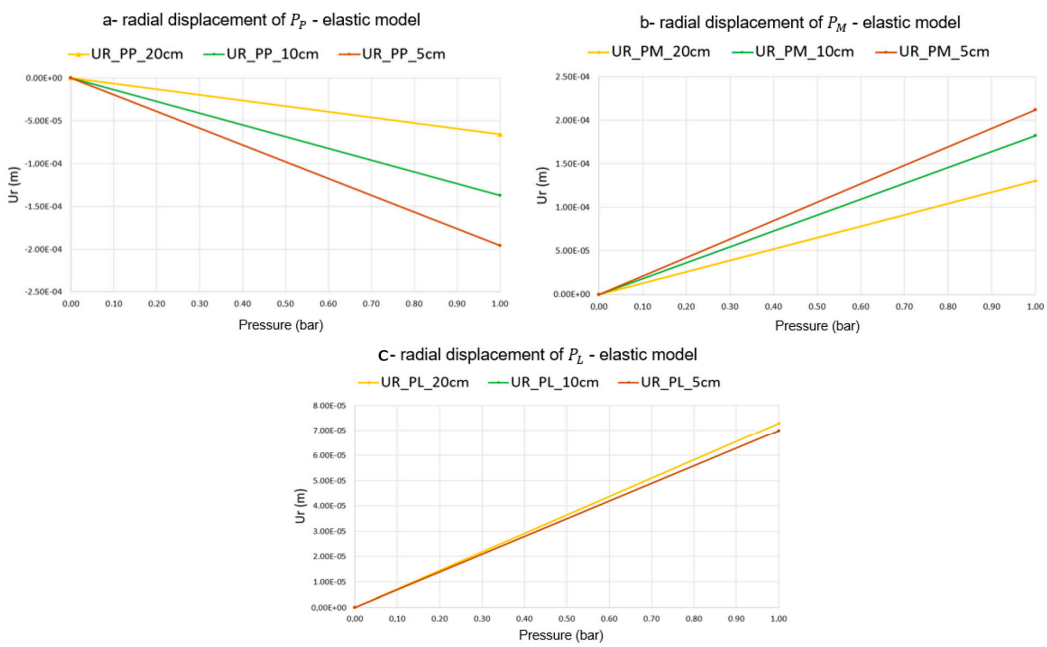

Figure 27. Radial displacements on the 3 post-processing points and for 3 mesh refinements—elastic model for concrete.

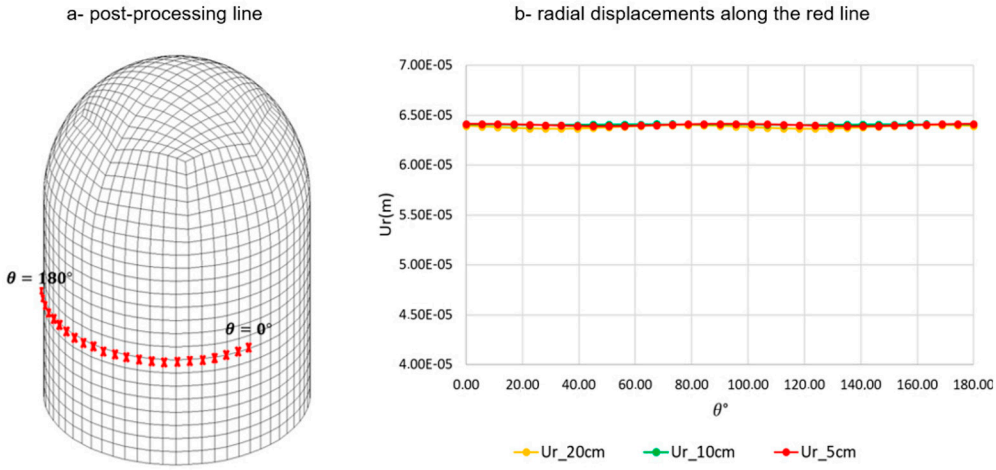

Figure 28. Radial displacements along the line z = 1.8 m—elastic model—structure with no opening.

3. Conclusions and Perspectives

The ASC (adaptive static condensation) method, first introduced in [18] and developed further in [21], offers a solution to the problem of reducing large structural problems to their expected nonlinear zone. By using the static condensation method [14] to eliminate degrees of freedom of the elastic domain, computational efforts can be focused solely on the nonlinear domain. The ASC method is particularly efficient when dealing with non-extended damage zones. However, the use of a uniform mesh in the whole structure throughout the calculation process limits its efficiency. This contribution presents an improved ASC method that utilizes an evolutionary mesh based on a uniform hierarchical mesh refinement of the DI. The efficiency of the new method was evaluated by studying a simplified reinforced concrete vessel subjected to internal pressure. Results obtained with the ASC method with mesh refinement consistently compared favorably with a standard complete calculation, with gain factors up to 14 obtained. Moreover, the ASC method with mesh refinement allows to carry out calculations with finesses inaccessible to cases run as complete calculations and to ASC cases without refinement. Further research is recommended to investigate more advanced adaptive mesh refinement techniques, requiring the integration of a robust projection technique for accurate projections in inelastic areas. This task can pose a significant challenge due to the complex behavior often exhibited in non-elastic zones, such as plasticity or damage, making field projection more difficult, especially considering potentially significant local variations. Data interpolation between mesh nodes can introduce errors, particularly when gradients are pronounced. Therefore, field projection algorithms must be numerically stable, especially in regions where material behavior is highly nonlinear. Accounting for these instabilities can be challenging when refining the mesh.

Author Contributions: Conceptualization, A.M., L.J., G.F. and L.D.; methodology, A.M., L.J., G.F. and L.D.; software, A.M., L.J., G.F. and L.D.; validation, A.M., L.J., G.F. and L.D.; formal analysis, A.M., L.J., G.F. and L.D.; investigation, A.M., L.J., G.F. and L.D.; resources, A.M., L.J., G.F. and L.D.; data curation, A.M., L.J., G.F. and L.D.; writing—original draft preparation, A.M.; writing—review and editing, A.M., L.J., G.F. and L.D.; visualization, A.M., L.J., G.F. and L.D.; supervision, A.M., L.J., G.F. and L.D.; project administration, A.M., L.J., G.F. and L.D.; funding acquisition, A.M., L.J., G.F. and L.D. All authors have read and agreed to the published version of the manuscript.

Funding: The project was funded by EDF R & D and CEA, tripartite institute agreement number 2020-F35158.

Data Availability Statement: Data are contained within the article.

Acknowledgments: The authors gratefully acknowledge the financial support contribution from EDF R&D for the development and the analysis of the simulation results.

Conflicts of Interest: The authors declare no conflict of interest.

References

1. Zenios, S.A. High-performance computing in finance: The last 10 years and the next. *Parallel Comput.* **1999**, *25*, 2149–2175. [CrossRef]
2. Bartels, C.; Breuer, M.; Wechsler, K.; Durst, F. Computational fluid dynamics applications on parallel-vector computers: Computations of stirred vessel flows. *Comput. Fluids* **2002**, *31*, 69–97. [CrossRef]
3. Gosselet, P.; Rixen, D.; Roux, F.-X.; Spillane, N. Simultaneous FETI and block FETI: Robust domain decomposition with multiple search directions. *Int. J. Numer. Methods Eng.* **2015**, *104*, 905–927. [CrossRef]
4. Farhat, C.; Roux, F. A method of finite element tearing and interconnecting and its parallel solution algorithm. *Int. J. Numer. Methods Eng.* **1991**, *32*, 1205–1227. [CrossRef]
5. Berger, M.J.; Oliger, J. Adaptive mesh refinement for hyperbolic partial differential equations. *J. Comput. Phys.* **1984**, *53*, 484–512. [CrossRef]
6. Berger, M.J.; Colella, P. Local Adaptive Mesh Refinement for Shock Hydrodynamics. *J. Comput. Phys.* **1989**, *82*, 184. [CrossRef]
7. Pewa, T.; Linde, T.; Weirs, V.G. *Adaptive Mesh Refinement—Theory and Applications*; Springer: Chicago, IL, USA, 2003.
8. Cheruvu, V. Multiresolution adaptive space refinement in geophysical fluid dynamics simulation. In *Adaptive Mesh Refinement—Theory and Applications*; Springer: Berlin/Heidelberg, Germany, 2005; pp. 161–170. [CrossRef]
9. Falle, S.A.E.G. AMR applied to non-linear Elastodynamics. In Proceedings of the Chicago Workshop on Adaptive Mesh Refinement Methods, Chicago, IL, USA, 3–5 September 2003.
10. Bergmans, J.; Keppens, R.; Van Odyck, D.E.A.; Achterberg, A. Simulations of Relativistic Astrophysical Flows. In Proceedings of the Chicago Workshop on Adaptive Mesh Refinement Methods, Chicago, IL, USA, 3–5 September 2003. [CrossRef]
11. Babuska, I.; Craig, A.; Mandel, J.; Pitkaranta, J. Efficient Preconditioning for the p-Version Finite Element Method in Two Dimensions. *SIAM J. Numer. Anal.* **1991**, *28*, 624–661. [CrossRef]
12. Craig, R.; Bampton, M. Coupling of Substructures for Dynamic Analyses. *AIAA J.* **2017**, *6*, 1313–1319. [CrossRef]
13. Santacreu, S.D. *Méthode de Raffinement de Maillage Adaptatif Hybride Pour le Suivi de fronts dans les Ecoulements Incompressibles*; Université Bordeaux I: Talence, France, 2006.
14. Guyan, R.J. Reduction of stiffness and mass matrices. *AIAA J.* **1965**, *3*, 380. [CrossRef]
15. Ong, J. Improved automatic masters for eigenvalue economization. *Finite Elem. Anal. Des.* **1987**, *3*, 149–160. [CrossRef]
16. Leung, A.Y. An accurate method of dynamic condensation in structural analysis. *Int. J. Numer. Methods Eng.* **1978**, *12*, 1705–1715. [CrossRef]
17. Lee, M.A. An Approach for Efficient, Conceptual-Level Aerospace Structural Design Using the Static Condensation Reduced Basis Element Method an Approach for Efficient, Conceptual-Level Aerospace Structural Design Using the Static Condensation. Ph.D. Thesis, School of Aerospace Engineering—Georgia Institute of Technology, Atlanta, GA, USA, 2018.
18. Llau, A.; Jason, L.; Dufour, F.; Baroth, J. Adaptive zooming method for the analysis of large structures with localized nonlinearities. *Finite Elem. Anal. Des.* **2015**, *106*, 73–84. [CrossRef]
19. Mezher, A.; Jason, L.; Folzan, G.; Davenne, L. Simulation of large dimensional reinforced and prestressed concrete structures using a new adaptive static condensation method including automatic mesh partitioning. *Finite Elem. Anal. Des.* **2022**, *202*, 103718. [CrossRef]
20. cast3m. 2023. Available online: http://www-cast3m.cea.fr/ (accessed on 18 February 2024).
21. Mezher, A. Amélioration des Performances Pour le Calcul des Structures à Comportement non Linéaire de Grandes Dimensions. Ph.D. Thesis, Université de Nanterre-Paris X, Nanterre, France, 2022.
22. Mazars, J. A description of micro- and macroscale damage of concrete structures. *Eng. Fract. Mech.* **1986**, *25*, 729–737. [CrossRef]
23. Pijaudier-Cabot, G.; Bazant, Z.P. Non Local Damage Theory. *Eng. Mech.* **1987**, *113*, 1512–1533. [CrossRef]
24. Zhang, R.; Li, L.; Zhao, L.; Tang, G. An adaptive remeshing procedure for discontinuous finite element limit analysis. *Int. J. Numer. Methods Eng.* **2018**, *116*, 287–307. [CrossRef]
25. Yue, P.; Zhou, C.; Feng, J.J.; Ollivier-Gooch, C.F.; Hu, H.H. Phase-field simulations of interfacial dynamics in viscoelastic fluids using finite elements with adaptive meshing. *J. Comput. Phys.* **2006**, *219*, 47–67. [CrossRef]
26. Lee, N.S.; Bathe, K.J. Error indicators and adaptive remeshing in large deformation finite element analysis. *Finite Elem. Anal. Des.* **1994**, *16*, 99–139. [CrossRef]
27. Wood, W.A.; Kleb, W.L. On Multi-dimensional Unstructured Mesh Adaption. In Proceedings of the 14th AIAA Computational Fluid Dynamics Conference on Multi-dimensional Unstructured Mesh Adaption, Norfolk, VA, USA, 28 June–1 July 1999. [CrossRef]
28. Bono, G.; Awruch, A.M. An adaptive mesh strategy for high compressible flows based on nodal Re-allocation. *J. Braz. Soc. Mech. Sci. Eng.* **2008**, *30*, 189–196. [CrossRef]
29. Gibert, G. *Propagation de Fissures en Fatigue par une Approche X-FEM avec Raffinement Automatique de Maillage*; Université de Lyon: Lyon, France, 2019.

30. Zienkiewicz, O.; Taylor, R.; Zhu, J. The hierarchical concept in finite element analysis. *Comput. Struct.* **1983**, *16*, 53–65. [CrossRef]
31. Verpeaux, P.; Charras, T. Multiplicateur de Lagrange, Condensation Statique et Conditions Unilatérales. In Proceedings of the 10e Colloque National en Calcul des Structures (CSMA), Giens, France, 9–13 May 2011.
32. Bérard, A. *Transferts de Champs Entre Maillages de Type Éléments Finis et Applications Numériques en Mécanique non Linéaire des Structures*; Université de Franche-Comté: Besançon, France, 2011.
33. Dureisseix, D.; Néron, D. A multiscale computational approach with field transfer dedicated to coupled problems. *Int. J. Multiscale Comput. Eng.* **2008**, *6*, 233–250. [CrossRef]
34. Lorentz, E.; Andrieux, S. Variational formulation for nonlocal damage models. *Int. J. Plast.* **1999**, *15*, 119–138. [CrossRef]
35. Giry, C.; Dufour, F.; Mazars, J. Stress-based nonlocal damage model. *Int. J. Solids Struct.* **2011**, *48*, 3431–3443. [CrossRef]
36. Costaz, J.L. Confinement. Enceintes. Technique de l'Ingénieur. 1997. Available online: http://www.techniques-ingenieur.fr/base-documentaire/energies-th4/conceptionconstruction-%0Aet-exploitation-des-reacteurs-nucleaires-42204210/confinement-enceintesb3290/ (accessed on 18 February 2024).
37. Mezher, A.; Jason, L.; Folzan, G.; Davenne, L. New adaptative static condensation method for the simulation of large dimensions prestressed reinforced concrete structures. In Proceedings of the International Conference on Computational Plasticity. Fundamentals and Application, Barcelona, Spain, 7–9 September 2021.

Disclaimer/Publisher's Note: The statements, opinions and data contained in all publications are solely those of the individual author(s) and contributor(s) and not of MDPI and/or the editor(s). MDPI and/or the editor(s) disclaim responsibility for any injury to people or property resulting from any ideas, methods, instructions or products referred to in the content.